International Journal of Heat and Mass Transfer 52 (2009) 822–838

Contents lists available at ScienceDirect

International Journal of Heat and Mass Transfer

journal homepage: www.elsevier.com/locate/ijhmt

Numerical studies on laminar natural convection inside inclined cylinders of unity aspect ratio

Vinoj Kurian [a], Mahesh N. Varma [a,b], A. Kannan [a,*]

[a] Department of Chemical Engineering, Indian Institute of Technology Madras, Chennai 600 036, India
[b] Department of Chemical Engineering, Indian institute of Science, Bangalore 560 012, India

ARTICLE INFO

Article history:
Received 5 November 2007
Received in revised form 2 June 2008
Available online 13 September 2008

Keywords:
Natural convection
Cylinder inclination
Flow patterns
Maximum convective velocity
Nusselt number
Critical Rayleigh number

ABSTRACT

The effect of cylinder inclination on thermal buoyancy induced flows and internal natural convective heat transfer is explored using CFD simulations. The cylinder's top and bottom surfaces were maintained at different temperatures while the curved surface was adiabatic. The aspect ratio (length/diameter) of the cylinder was unity and the Prandtl number of the fluid was fixed at 0.71. The Rayleigh number of the confined fluid was varied from 10^3 to 3.1×10^4 by changing the specified end wall temperatures. The critical Rayleigh number was estimated to be 3800 for the vertical cylinder. Relaxing the convergence criterion caused false hysteresis in the converged results for the vertical cylinder. Typical natural convective fluid flow and temperature patterns obtained under laminar flow conditions are illustrated for various inclinations ranging from 0° to 180°. Flow visualization studies revealed complex three-dimensional patterns. Different thermal–hydrodynamic regimes were identified and were classified in terms of Rayleigh number and angle of inclination. Empirical correlations for the Nusselt number and maximum velocities in the domain as a function of the inclination angle and Rayleigh number are developed.

1. Introduction

Natural convection induced by thermal buoyancy effects in a gravitational force field is observed in many applications. These include electronic components design, crystal growth configurations, air conditioning of buildings, design of storage of hot fluids in solar power plants and food sterilization [1–4]. Inclination of containers filled with fluid, inside which convective heat or mass transfer occur, may have either desirable or undesirable effects depending on the application. Effects of inclination on heat transfer have been explored in practical applications involving solar energy heaters and double glazed windows. However, there are certain applications where undesirable mixing in fluids is inadvertently caused even by slight inclination of a vertical column [5]. These include tracer studies and mass transfer in vertical columns where unstable density gradients may lead to higher axial mixing [6].

Ozoe et al. [7], Arnold et al. [8], Schinkel [9] and Soong et al. [10] have for instance, studied the effect of inclination on square/rectangular bodies. Both laminar and turbulent convection was studied by Kuyper et al. [11] in square cavities inclined between 0° and 180°. The Rayleigh number was varied between 10^4 and 10^{11}. However, only limited information exists for the effect of inclination angle on natural convective heat transfer inside cylindrical enclosures. Bontoux et al. [12] studied the influence of inclining the cylinder on the flow structures. In their work, the height to diameter ratio (aspect ratio) of the cylinder was kept at 5 and the cylinder's lateral walls were taken to be perfectly conducting. Heiss et al. [13] described a numerical code that was developed to calculate both transient and steady state natural three-dimensional convection occurring inside cylindrical enclosures.

Neumann [14] studied three-dimensional natural convection in vertical cylinders including those of unity aspect ratio. He recommended numerical simulations for determining fluid flows at Rayleigh numbers much higher than the critical. Crespo del Arco et al. [15] investigated steady and oscillatory convection in vertical cylinders at different aspect ratios including that of unity. Schneider and Straub [16] investigated laminar natural convection in cylinders of varying inclinations and adiabatic curved wall in a three-dimensional numerical study. Muller et al. [17] studied natural convection in vertical Bridgman configurations taking into account the influence of aspect ratio, Rayleigh number and Prandtl number.

2. Scope of the current study

This study involves laminar natural convection in a fluid-filled cylinder of unity aspect ratio with different specified end wall temperatures and adiabatic curved wall. Unity aspect ratio of the cylinder was considered as a starting point for our detailed investigations on the effects of inclination on convergence behaviour of

* Corresponding author. Tel.: +91 44 2257 4170; fax: +91 44 2257 0509.
E-mail address: kannan@iitm.ac.in (A. Kannan).

0017-9310/$ - see front matter © 2008 Elsevier Ltd. All rights reserved.
doi:10.1016/j.ijheatmasstransfer.2008.06.041

Nomenclature

C_p	specific heat of the liquid in the can (J kg^{-1} K^{-1})
D	diameter of the cylinder (m)
Fo	Fourier number
g	gravitational acceleration constant (m s^{-2})
k	thermal conductivity of the liquid in the can (W m^{-1} K^{-1})
K	dimensionless axial temperature gradient at the center of the cylinder
K_{WALL}	dimensionless axial temperature gradient at the adiabatic wall of the cylinder
L	length of the cylinder (m)
Nu	Nusselt number
Nu_{loc}	local Nusselt number
p	pressure (Pa)
Pr	Prandtl number
$\bar{q}$	area averaged wall heat flux (W/m^2)
q_k	conduction heat flux (W/m^2)
q_z^*	dimensionless convective axial heat flux
r	radial distance (m)
R	radius of the cylinder (m)
Ra	Rayleigh number
Ra_c	critical Rayleigh number
Ra_K	transition Rayleigh number
Ra_{rv}	reduced Rayleigh number for the vertical cylinder
Ra_{ri}	reduced Rayleigh number for the inclined cylinder
t	time (s)
T	temperature (K)
T_{cold}	cold surface temperature (K)
T_{hot}	hot surface temperature (K)
T_{ref}	reference temperature (K)
T_*	scaled temperature
ΔT	temperature difference between hot and cold walls (K)
V	velocity (m s^{-1})
V_{max}	maximum velocity (m s^{-1})
$V_{d,max}$	dimensionless maximum velocity
w_d	dimensionless axial velocity
z	axial distance (m)

Greek symbols

α	angle of inclination of cylinder from vertical (°)
α_T	thermal diffusivity (m^2 s^{-1})
β	thermal expansivity (K^{-1})
θ	azimuthal angle
μ	viscosity (Pa s)
ρ	density (kg m^{-3})
ρ_{ref}	density at reference temperature (kg m^{-3})
ν	kinematic viscosity (m^2 s^{-1})
ϕ	angle of inclination from vertical (rad)

Subscripts

c	critical
d	dimensionless
max	maximum
min	minimum
r	reduced
ref	reference

Superscript

*	scaled

numerical simulations, fluid flow patterns, flow regimes and Nusselt numbers. Transition in stability and symmetry of the flow patterns are also observed to occur in numerical simulations for a vertical cylinder when the aspect ratio increases from fractional values to $\geqslant 1$ [16,17]. Schneider and Straub [16] performed numerical calculations using a coarse mesh in order to focus more on parameter dependencies and to economize computing costs. These authors did not identify different flow regimes in their study. With advances in computer speed and memory, the complex flow and temperature fields may be captured accurately using a finer mesh.

Commercial CFD software is used to perform mesh independent numerical simulations of the governing transport equations. The critical Rayleigh number at which the onset of convection occurs in a vertical cylinder is also estimated. Three-dimensional flow patterns for vertical and inclined cylinder are presented. The relationship between convective flow and its effect on heat transfer is examined. Simple correlations are proposed for predicting the effect of inclination on the Nusselt number and maximum velocity in different regimes. Further, the dynamics associated with the onset of natural convection are examined through transient simulations at different Rayleigh numbers.

3. Problem specifications

Air with a Prandtl number of 0.71, confined in a cylinder with unity aspect ratio and inclined between 0° and 180° with respect to the vertical was considered in this work. The Rayleigh number (Ra) investigated varied between 10^3 and 3.1×10^4. The properties of air at a reference temperature of 25 °C chosen in this work are given in Table 1. The cylinder length was fixed at 2.2×10^{-2} m and the aspect ratio (L/D) was fixed at unity. The Rayleigh number could be then varied according to the imposed temperature difference. The parameter values were in conformity to those taken by Schneider and Straub [16]. The hot plate is located at the bottom while the cold plate is at the top for an inclination angle of 0° while the opposite is applicable for an inclination angle 180°. A schematic sketch of the geometry studied is shown in Fig. 1.

The flow is considered laminar owing to the relatively low Rayleigh numbers investigated [15–17]. The onset of convection in cylinders of diameter comparable to the length or lower will be delayed due to viscous damping offered by the vertical wall which in turn will increase the critical Rayleigh number. In Schneider and Straub's [16] work, the range of parameters investigated using the laminar flow model were Rayleigh number ($Ra < 8 \times 10^4$), Prandtl number (>0.7), aspect ratio (L/D: 0.5–2), and inclination angle (0–180°). They suggested that their correlation may be extended for Prandtl numbers greater than 0.7 due to a weak effect of Prandtl number on Nusselt number beyond this value. Muller et al. [17] observed an extreme extension of the laminar convective range for the unity aspect ratio case. Transition to turbulence in this case was observed at around

Table 1
Properties of air at 25 °C

Serial number	Property	Value
1	Density (ρ)	1.185 kg/m^3
2	Viscosity (μ)	1.831×10^{-5} Pa s
3	Thermal conductivity (k)	2.61×10^{-2} W/(m K)
4	Specific heat (C_p)	1.0044×10^3 J/(kg K)
5	Thermal expansivity (β)	0.003356 K^{-1}
6	Thermal diffusivity ($\alpha_T = k/(\rho C_p)$)	2.2×10^{-5} m^2/s
7	Kinematic viscosity ($\nu = \mu/\rho$)	1.55×10^{-5} m^2/s
8	Prandtl number ($Pr = C_p\mu/k$)	0.71

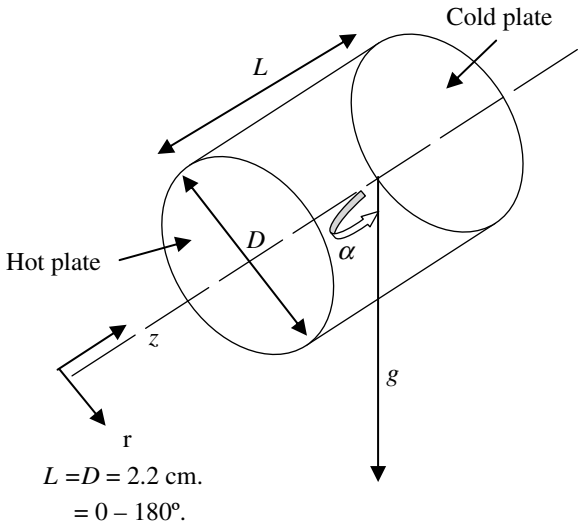

Fig. 1. Configuration of the cylindrical system under study.

4.64×10^5 when water (Prandtl number = 6.7) was the fluid studied. Gallium, for which the Prandtl number was very low at 0.02, exhibited the onset of turbulence at 6.86×10^4. Both these values are higher than the maximum Rayleigh number of 3.1×10^4 studied in this work for a Prandtl number fluid of 0.71. A detailed experimental study by Heslot et al. [18] on cylinders with unity aspect ratio and adiabatic curved wall revealed a transition to soft turbulence at a Rayleigh number of 10^5 while hard turbulence was attained at 10^7. These Rayleigh numbers are one to three orders of magnitude higher than the values considered in this study. In a recent study [19] on inclined cylinders with adiabatic sidewalls and aspect ratio of 9, the Rayleigh number based on length was in the order of 10^7. Laminar flow model was applied with estimated Nusselt numbers varying from 1 to 200. Studies in the literature on inclined square cavities have used the laminar flow model until a *Ra* value of 10^6 and the turbulent flow model for *Ra* values in the order of 10^{10} [5]. The Nusselt numbers at *Ra* value of 10^6 were between 7 and 10 over the entire range of inclinations. In turbulent flow, the Nusselt numbers were in the order of 100. Cianfrini et al. [20] studied the effects of tilting on natural convection in square cavities containing air and considered laminar flow in the Rayleigh number range of 10^4-10^6. In this range, the mean Nusselt numbers varied from 4 to 12. Jahnke et al. [21] studied two-dimensional natural convection in a horizontally oriented container of unity aspect ratio with temperature distributions on the sidewalls. They extended the laminar studies until a Rayleigh number of 2×10^5 and the Nusselt numbers were in the range of 2–5. D'Orazio et al. [22] studied rectangular enclosures with adiabatic sidewalls and applied laminar flow until a maximum Rayleigh number of 2×10^6. The aspect ratio in their case varied from 2 to 6. From the above, the choice of laminar flow for the present set of simulations for *Ra* not exceeding 3.1×10^4 is justified.

4. Governing transport equations and boundary conditions

The software CFX v10 [23] was used to solve the governing continuity, momentum and energy equations for the defined geometry and associated boundary conditions. The domain was defined in the global co-ordinate frame in which the solver carries out the calculations. The generalized transport equations solved are given below.

4.1. The continuity equation

$$\frac{\partial \rho_{\mathrm{ref}}}{\partial t} + \frac{1}{r}\cdot\frac{\partial}{\partial r}(\rho_{\mathrm{ref}} r v_{\mathrm{r}}) + \frac{1}{r}\cdot\frac{\partial}{\partial \theta}(\rho_{\mathrm{ref}} v_\theta) + \frac{\partial}{\partial z}(\rho_{\mathrm{ref}} v_z) = 0 \tag{1}$$

4.2. The momentum equation

r-component

$$\rho_{\mathrm{ref}}\left(\frac{\partial v_{\mathrm{r}}}{\partial t} + v_{\mathrm{r}}\frac{\partial v_{\mathrm{r}}}{\partial r} + \frac{v_\theta}{r}\frac{\partial v_{\mathrm{r}}}{\partial \theta} + v_z\frac{\partial v_{\mathrm{r}}}{\partial z} - \frac{v_\theta^2}{r}\right) = -\frac{\partial p}{\partial r} + \mu\left[\frac{\partial}{\partial r}\left(\frac{1}{r}\frac{\partial}{\partial r}(r v_{\mathrm{r}})\right) + \frac{1}{r^2}\frac{\partial^2 v_{\mathrm{r}}}{\partial \theta^2} + \frac{\partial^2 v_{\mathrm{r}}}{\partial z^2} - \frac{2}{r^2}\frac{\partial v_\theta}{\partial \theta}\right] + \rho g_{\mathrm{r}} \tag{2}$$

θ-component

$$\rho_{\mathrm{ref}}\left(\frac{\partial v_\theta}{\partial t} + v_{\mathrm{r}}\frac{\partial v_\theta}{\partial r} + \frac{v_\theta}{r}\frac{\partial v_\theta}{\partial \theta} + v_z\frac{\partial v_\theta}{\partial z} + \frac{v_{\mathrm{r}} v_\theta}{r}\right) = -\frac{1}{r}\frac{\partial p}{\partial \theta} + \mu\left[\frac{\partial}{\partial r}\left(\frac{1}{r}\frac{\partial}{\partial r}(r v_\theta)\right) + \frac{1}{r^2}\frac{\partial^2 v_\theta}{\partial \theta^2} + \frac{\partial^2 v_\theta}{\partial z^2} + \frac{2}{r^2}\frac{\partial v_{\mathrm{r}}}{\partial \theta}\right] + \rho g_\theta \tag{3}$$

z-component

$$\rho_{\mathrm{ref}}\left(\frac{\partial v_z}{\partial t} + v_{\mathrm{r}}\frac{\partial v_z}{\partial r} + \frac{v_\theta}{r}\frac{\partial v_z}{\partial \theta} + v_z\frac{\partial v_z}{\partial z}\right) = -\frac{\partial p}{\partial z} + \mu\left[\frac{1}{r}\frac{\partial}{\partial r}\left(r\frac{\partial v_z}{\partial r}\right) + \frac{1}{r^2}\frac{\partial^2 v_z}{\partial \theta^2} + \frac{\partial^2 v_z}{\partial z^2}\right] + \rho g_z \tag{4}$$

4.3. The energy equation

$$\rho_{\mathrm{ref}} C_p\left(\frac{\partial T}{\partial t} + v_{\mathrm{r}}\frac{\partial T}{\partial r} + \frac{v_\theta}{r}\frac{\partial T}{\partial \theta} + v_z\frac{\partial T}{\partial z}\right) = k\left[\frac{1}{r}\frac{\partial}{\partial r}\left(r\frac{\partial T}{\partial r}\right) + \frac{1}{r^2}\frac{\partial^2 T}{\partial \theta^2} + \frac{\partial^2 T}{\partial z^2}\right] \tag{5}$$

Viscous dissipation effects are neglected due to low viscosity of the system. Applying the Boussinesq approximation, the density in the body force term is given by

$$\rho = \rho_{\mathrm{ref}}[1 - \beta(T - T_{\mathrm{ref}})] \tag{6}$$

4.4. Boundary conditions

The top and bottom surface temperatures of the cylinder were kept at isothermal conditions of T_{hot} and T_{cold}, respectively, i.e.

$$T(r,\theta,0) = T_{\mathrm{hot}} \quad T(r,\theta,L) = T_{\mathrm{cold}} \tag{7}$$

The curved wall is considered to be adiabatic

$$\left.\frac{\partial T}{\partial r}\right|_{r=R} = 0 \tag{8}$$

No slip boundary conditions applied at the top, side and bottom stationary walls where the velocities are 0. The reference temperature (T_{ref}) was taken as the arithmetic mean of the hot and cold wall temperatures.

5. Mesh and solver details

The problem domain is resolved into volume meshes, whose dimensions play an important role in determining the accuracy of the converged numerical simulations. In order to resolve

accurately the rapid velocity and temperature variations near the wall, the meshes here were made much finer relative to those in the core region. The unstructured mesh option was used which involves prismatic elements near the wall and tetrahedral elements in the core. Using tetrahedral elements throughout would have entailed prohibitively fine meshes for the required accuracy. Flat prismatic wedge shaped elements were placed close to the walls as shown in Fig. 2. An inflation parameter of 10 layers with a geometric expansion factor of 1.3 was chosen. This arranged the prismatic elements from the wall surface in a sequence of 10 layers of gradually increasing thickness. These ensured an adequate number of elements near the wall and avoided a sudden jump in mesh size. The results are found to be mesh-independent under these conditions. The total number of elements was 4.33×10^5 that included 3.06×10^5 tetrahedral nodes and 1.27×10^5 wedges. This fine mesh resulted in each run taking around 40 min for completion in a Pentium P-IV machine of 3.80 GHz speed.

The CFX software involves the finite volume method. It uses an unstaggered collocated grid to overcome the decoupling of pressure and/or velocity. The problems associated with checker board type of oscillations of pressure and velocity that are associated with collocated meshes were overcome by using a robust interpolation scheme similar to that used by Rhie and Chow [24]. A coupled solver is used in which the hydrodynamic equations for velocity and pressure are solved as a single system. A multi-grid technique based on successive solutions in fine and coarse grid schemes is used to accelerate the incomplete lower upper factorisation technique for solving the set of linearized equations. CFX has optional schemes such as first-order upwind difference and numerical advection with specified blend factor. The blend factor can be varied between 0 and 1 to opt between the first- and second-order schemes to control numerical diffusion. The high resolution scheme option was chosen which maintains the blend factor as close as possible to 1 without violating the boundedness principle. In the present simulations non-physical overshoots or undershoots in the solution were not encountered. The convergence criterion was based on specifying the normalized r.m.s. residuals to less than 10^{-6} which from a CFX point of view is very tight. The residuals were normalized by dividing the control volume imbalance with a term proportional to the representative range of the variable in the domain. These normalized residuals are independent of initial guess.

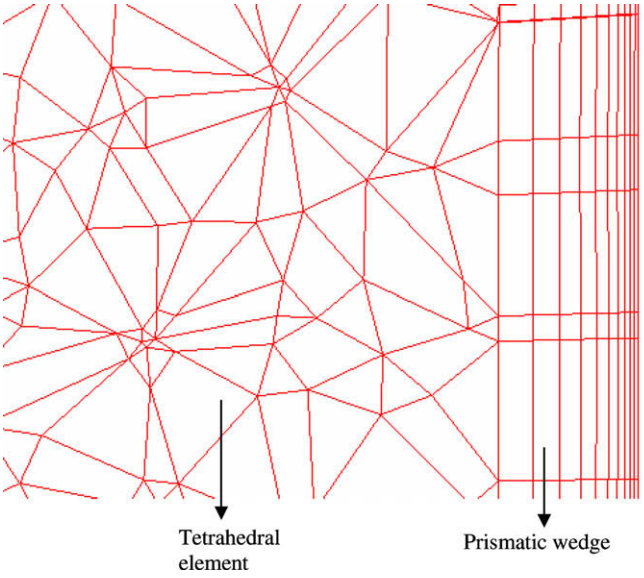

Fig. 2. Mesh inflation view.

For the range of variables investigated in this study as given in Table 1 corresponding to a Rayleigh number range of 10^3–3.1×10^4, the solutions were found to be steady. For a fluid of Prandtl number 0.02 and cylinder with unity aspect ratio, Crespo del Arco et al. [15] found solutions to be steady until a Rayleigh number of 3.2×10^4. For a fluid with Prandtl number of 6.7, Muller et al. [17] found that their transient simulations up to a Rayleigh number of 50,000 reached steady state in about 0.6 s. A typical transient simulation in the present study shows that the cylinder inclined at 45° attains a steady solution at the maximum Rayleigh number of 31,024 in 5 s. Schneider and Straub [16] reported steady state results over the entire range of inclination angles (0–180°) and Rayleigh numbers up to 80,000 with a fluid having Prandtl number of 0.68.

6. Apparent hysteresis behaviour in Nusselt number for the vertical cylinder

A peculiar behaviour was observed when the r.m.s. residuals were specified at a setting of 10^{-4} which is usually considered sufficient from an engineering viewpoint for most simulations [23]. Simulations for the vertical cylinder were first carried sequentially in the direction of increasing Rayleigh numbers and then in the direction of decreasing Rayleigh numbers. The converged results of the previous simulation were used as initial guesses for the next simulation. Surprisingly, the simulation results showed significant differences over a certain range of Rayleigh numbers depending on whether the simulations were carried out in the forward or backward direction. This is illustrated in Fig. 3 where the surface area averaged Nusselt number estimates are plotted as a function of Rayleigh number. The local Nusselt number is defined as follows:

$$Nu_{\mathrm{loc}} = -\left.\frac{\partial \frac{(T - T_{\mathrm{cold}})}{(T_{\mathrm{hot}} - T_{\mathrm{cold}})}}{\partial\left(\frac{z}{L}\right)}\right|_{z=0} \tag{9}$$

This hysteresis behaviour was closely examined. For simulations carried out in the backward direction, the critical Rayleigh number was observed at 3800 which matches well with the values reported in the literature. However, in the forward direction, the conduction heat transfer trend characterized by a linear axisymmetric temperature profile and unity Nusselt number persisted even until a Rayleigh number of 6800. While proceeding in the forward direction, the CFD simulation convergence patterns showed a peculiar trend at lower Rayleigh numbers. The r.m.s. residuals decreased

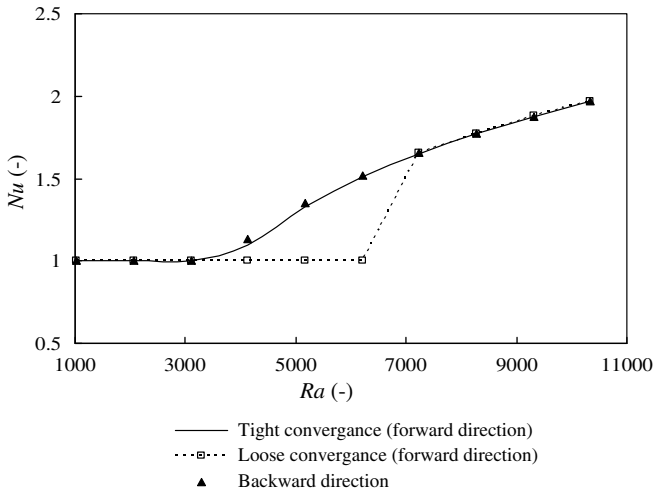

Fig. 3. Importance of tight convergence specification on critical Rayleigh number predictions.

rapidly and apparent convergence to a conduction solution was indicated early with a relaxed convergence criterion. Using a tighter convergence criterion, the r.m.s. residuals showed a subsequent *increase* after a certain number of iterations, followed by an eventual monotonic decrease below the specified convergence criterion. The simulations were allowed to continue for many more iterations to ensure that there was no further subsequent increase in the residuals. Convergence was ensured by monitoring the variation of temperature and velocity at some pre-defined monitor points where the temperature gradients and velocity gradients were significant. Results showed that with strict convergence criterion, there were no subsequent significant changes in variable values with further iterations. The apparent hysteresis trend did not occur in the case of inclined cylinders. Mesh independency studies were also conducted to confirm the accuracy of the solution. An even finer mesh with 7.83 lakhs elements was used and the results were in good agreement with the previous simulation results of 4.33 lakhs elements mesh. This is shown in Fig. 4a for a typical case of a cylinder inclined at 45° over the range of *Ra* studied and in Fig. 4b over the range of inclination angles studied at a given *Ra*.

Wang and Hamed [25] observed hysteresis in Nusselt number variation with inclination angle, in an inclined rectangular enclosure of aspect ratio (height/width) of 0.25. However, in the present case, involving a higher aspect ratio, no hysteresis was observed in Nusselt number when the inclination angle was changed from 0° to 180° in either the forward or backward directions.

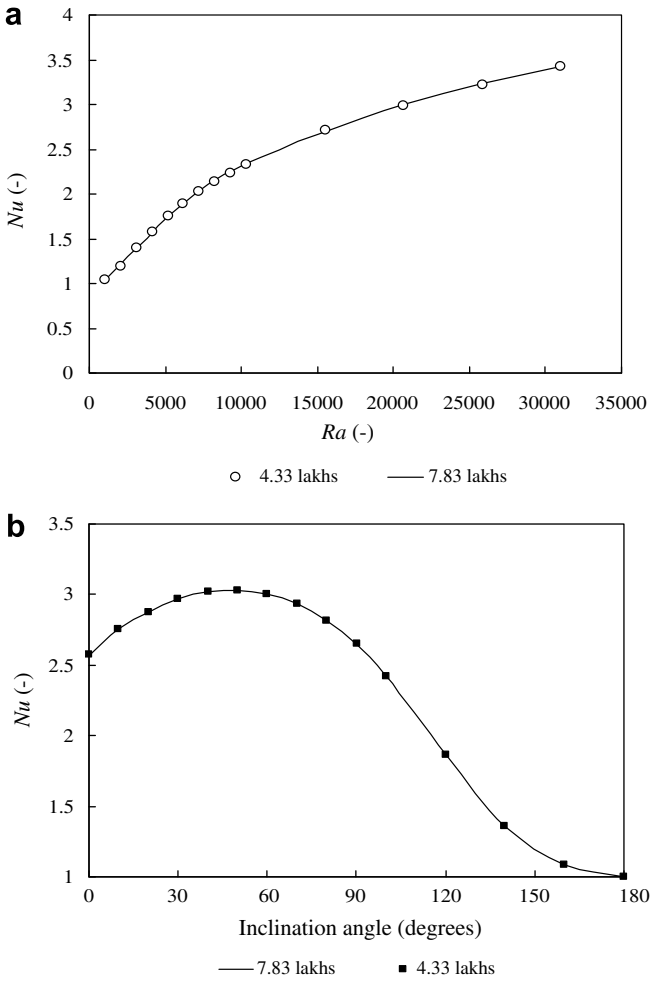

Fig. 4. Mesh independency studies based on Nusselt numbers. (a) Cylinder inclined at 45° at different Rayleigh numbers; and (b) cylinder at a fixed *Ra* = 21,500 and different inclination angles.

7. Estimation of critical Rayleigh number (Ra_c) for the vertical cylinder

Critical Rayleigh number for the vertical cylinder was estimated with the technique used by Schneider and Straub [16]. The steady state results corresponding to a 0.2° inclination were provided as initial guesses for the vertical cylinder and transient simulations were carried out for different Rayleigh numbers. The velocity in the domain died quickly to very low values for sub critical Rayleigh numbers while for the critical *Ra* of 3800, it remained constant after an initial decrease. For supercritical Rayleigh numbers, the velocities decreased and then increased. Since a 0.5 °C change in temperature difference caused a Rayleigh number change of 500, further refinement was not numerically justified. The estimated critical Rayleigh number was next compared with values reported in the literature.

Charlson and Sani [26] studied the onset of axisymmetric convection in cylinders over a wide range of aspect ratios. They completed their linear stability analysis in a subsequent study [27] for non-axisymmetric flows. The equations governing the dynamics of the system were recast in a variational formulation and the Rayleigh Ritz technique was applied to approximate the solution. For a unity aspect ratio, their analyses predict $Ra_c \approx 4500$ for the non-axisymmetric mode. Other numerical evidences in the literature for the vertical cylinder's critical Rayleigh number with adiabatic curved wall and unity aspect ratio are summarized below.

(a) Crespo del Arco et al. [15] identified the critical Rayleigh number as 3776 from numerical calculations based on the finite difference method.
(b) Schneider and Straub [16] observe Ra_c of ≈4300 (with a coarse mesh using finite difference method).
(c) Buell and Catton [28] identified a critical Rayleigh number of 3800 using the Galerkin method.

Transient simulations were also carried out to further verify the critical Rayleigh number as well as record the dynamics occurring before the attainment of steady state. The second-order backward Euler scheme was adopted in the transient simulations. This scheme is robust, implicit and did not show any non-physical overshoots or undershoots during the course of the simulation runs. Three-dimensional transient simulations were carried out for different Rayleigh numbers ranging from 3500 to 9308 until the solutions reached their respective steady states. Typical results are shown in Fig. 5. The simulations were,

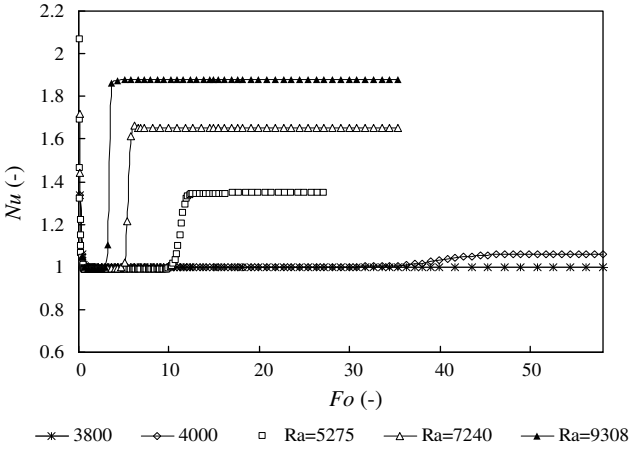

Fig. 5. Transient Nusselt numbers as a function of Rayleigh number.

however, numerically expensive as the time taken to reach steady state was high especially at lower Rayleigh numbers. The time stepping increments were kept at 0.1 s. The transient simulation results show good agreement with the critical Rayleigh number value calculated above. For instance, the convection was absent for $Ra = 3500$, barely discernible at $Ra = 3800$, when the Nusselt number value just exceeded unity. At $Ra = 4000$, the convection though weak was clearly evident. Initially, the Nusselt numbers were very high due to high thermal gradients across small conduction layer thickness in the domain. As the temperature gradient gradually gets established across the entire domain, the Nusselt number values decreased to unity implying motionless conduction mode of heat transfer. The conduction solution for heat transfer appeared to persist for a significant duration during which period the velocity values gradually increased. Once the velocities have increased a sufficient magnitude, the Nusselt numbers began increasing towards their eventual steady state values depending on the Rayleigh number. During this period, the linearly stratified temperature contours began to slowly distort indicating the onset of convection. The temperature contour plots during the various phases of: (a) initial development, (b) conduction, (c) incipient convection, and (d) steady state convection at a representative Rayleigh number of 5275 are given in Fig. 6.

The time taken by the fluid in the vertical cylinder to reach the intermediate unity Nusselt number state appears to be nearly the same for all Rayleigh numbers. The total time taken by the system to reach the eventual steady state convection mode, however, varies with Rayleigh number. At higher Rayleigh numbers, the final steady state is attained quicker than at lower Rayleigh numbers. Further, the time taken for the transition from the trivial intermediate quasi-steady-state to the final steady state varies with Rayleigh number as well. The transition time is more at lower Rayleigh numbers whereas a relatively quick transformation is evident at higher Rayleigh numbers.

8. Flow patterns for various angles of inclination

For the vertical cylinder of unity aspect ratio, the flow patterns were in qualitative agreement with those reported in previous studies [14,16,17]. Over a wide range of Rayleigh numbers (4000–80,000) the non-axisymmetric flow pattern was found to constitute the stable mode. The fluid ascends in one half of the plane and descends in the other half. In the principal plane ($\theta = 0, \pi$), the vector plot reveals a single inclined roll while in the plane orthogonal to the principal plane ($\theta = \pi/2, 3\pi/2$), four rolls were seen. For the range of Rayleigh numbers studied in this work, two additional rolls in the principal plane were also observed. However, a detailed visualization and description on the three-dimensional flow patterns are only limited in the literature as for e.g. Crespo del Arco and Bontoux [29] and Bontoux et al. [30]. In the study by Crespo del Arco and Bontoux [29], the complicated three-dimensional flows for a vertical cylinder with conducting sidewalls and an aspect ratio of 2 were presented. Bontoux et al. [30] describe the flow patterns in a horizontal cylinder with conducting sidewalls and a higher aspect ratio of 5. We summarize the important features of the three-dimensional flow patterns obtained in the present study for typical cases (0°, 45°, 90° and 150°) at the maximum investigated Rayleigh number of 31,027.47. The 3-D flow patterns obtained from CFX post-processor represent the paths taken by a particle of zero mass driven by the vector field [23].

8.1. Vertical cylinder

The principal plane $(0, \pi)$ was found to divide the flow domain into two halves. At a location close to the bottom right corner of the wall, corresponding to about 90% of the radius, and at about 6% of vertical height, secondary loops that are counter rotating relative to the primary central loops are formed (Fig. 7a). Fluid exits almost perpendicularly outwards from the secondary loop and

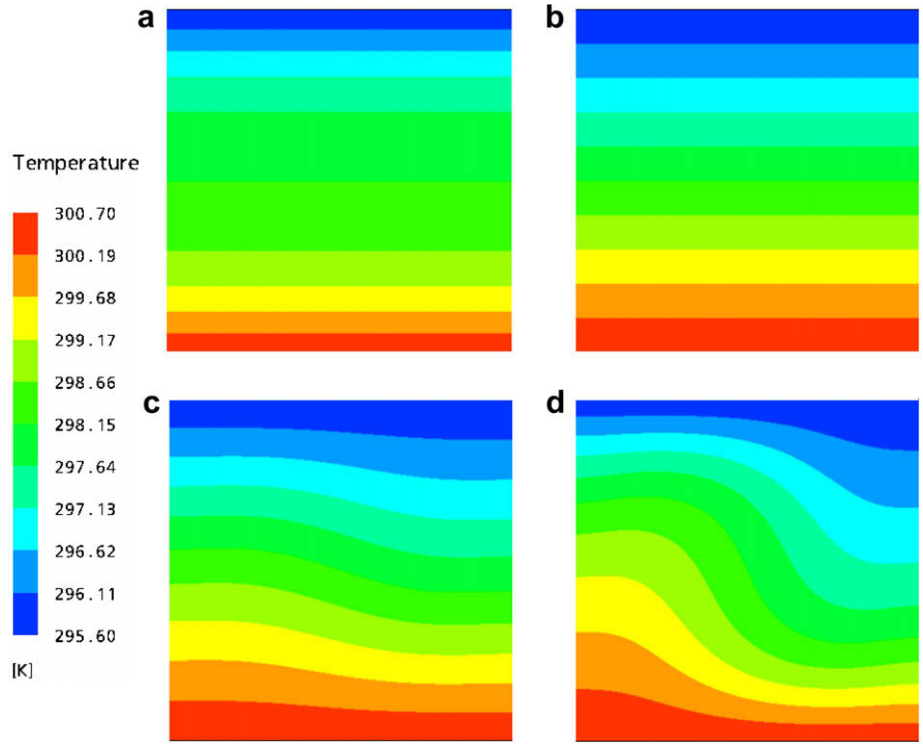

Fig. 6. Temperature contours in the vertical mid plane at $Ra = 5275$. (a) $Fo = 0.11$, (b) $Fo = 5.4$, (c) $Fo = 10.5$, and (d) $Fo = 16.3$.

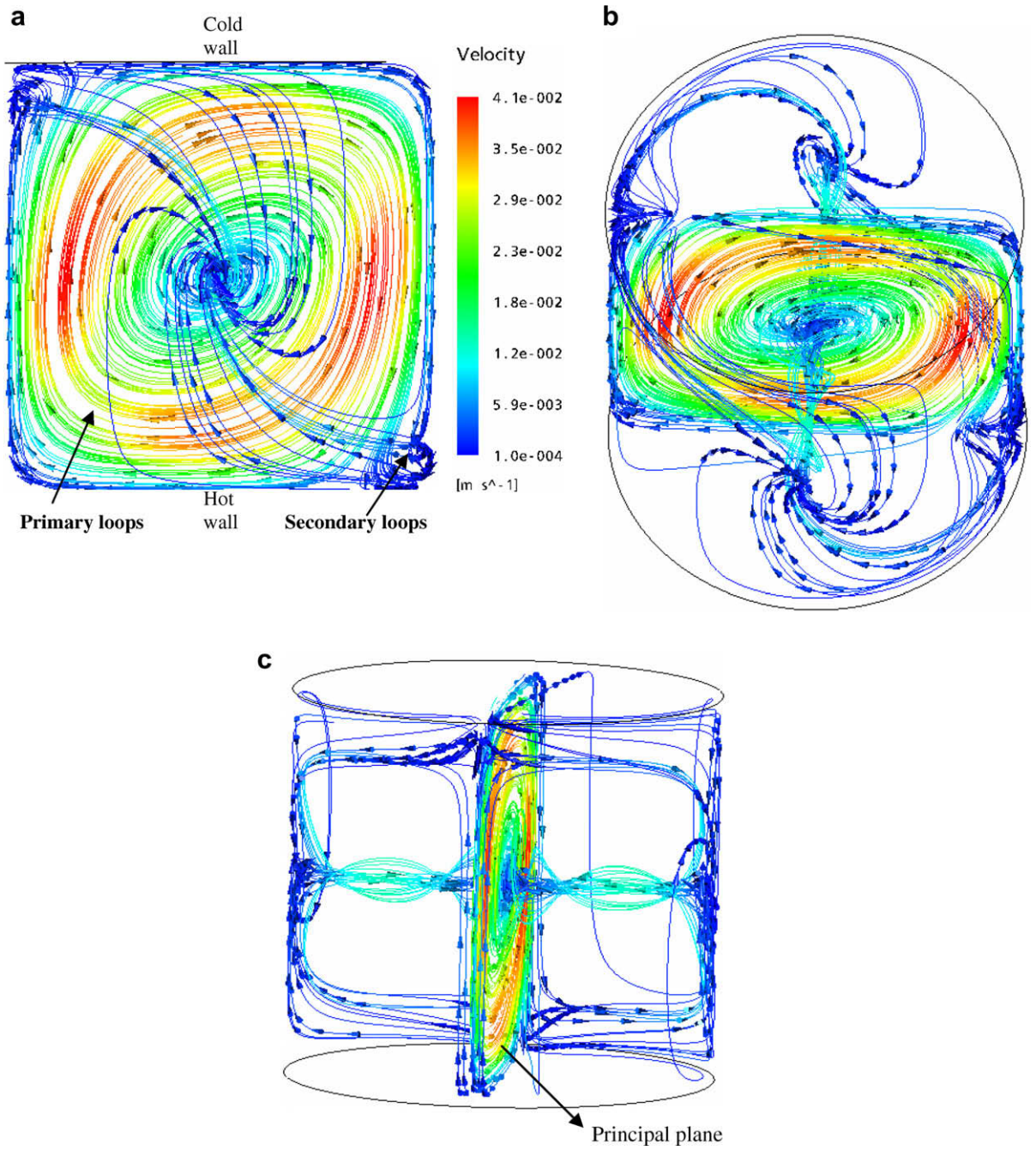

Fig. 7. Flow patterns for the vertical cylinder at $Ra = 31027.47$. (a) Front view, (b) top view, and (c) side view.

moves upwards (Fig. 7b). A similar occurrence takes place at the top left corner and the fluid moves downwards. The streams that had left the principal plane from the top left corner and bottom right corner secondary vortex zones, converge at mid-height of the curved wall and subsequently coil towards the centre and create the inner loops on the principal plane (Fig. 7a and c). As shown in Fig. 7a and b, the expanding central inner loops on the principal plane, lead to streams leaving from the top and bottom edges. The streams that leave at the bottom and top edges from the inner (primary) loop of the principal plane are deflected by the curved wall and move upward or downward (depending on whether they originated from the bottom or top region of the principal plane). These streams ascend/descend to some distance and then move towards the principal plane in a spiralling manner. This contributes to the outward and inward flows on the orthogonal plane. The flow patterns did not show a qualitative change in the Rayleigh number range investigated.

8.2. Cylinder inclined at 45°

The three-dimensional flow patterns are illustrated in Fig. 8. The distinct features for this inclination angle relative to the vertical case are: (a) higher velocities in the domain, (b) absence of secondary loops at the top left and bottom right corners, and (c) loops that are stretched in the principal plane at the centre.

8.3. Horizontal cylinder (90° inclination)

The flow patterns in a horizontal cylinder are distinguished by occurrence of two loops at the centre (Fig. 9a). For clarity only a

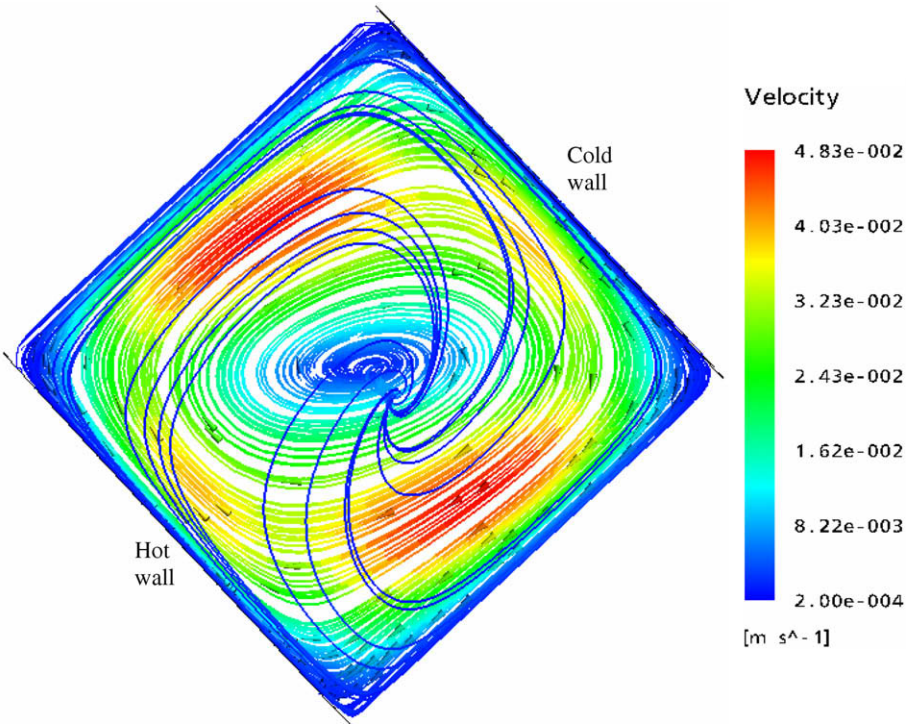

Fig. 8. Flow patterns in a cylinder inclined at 45° for $Ra = 31027.47$.

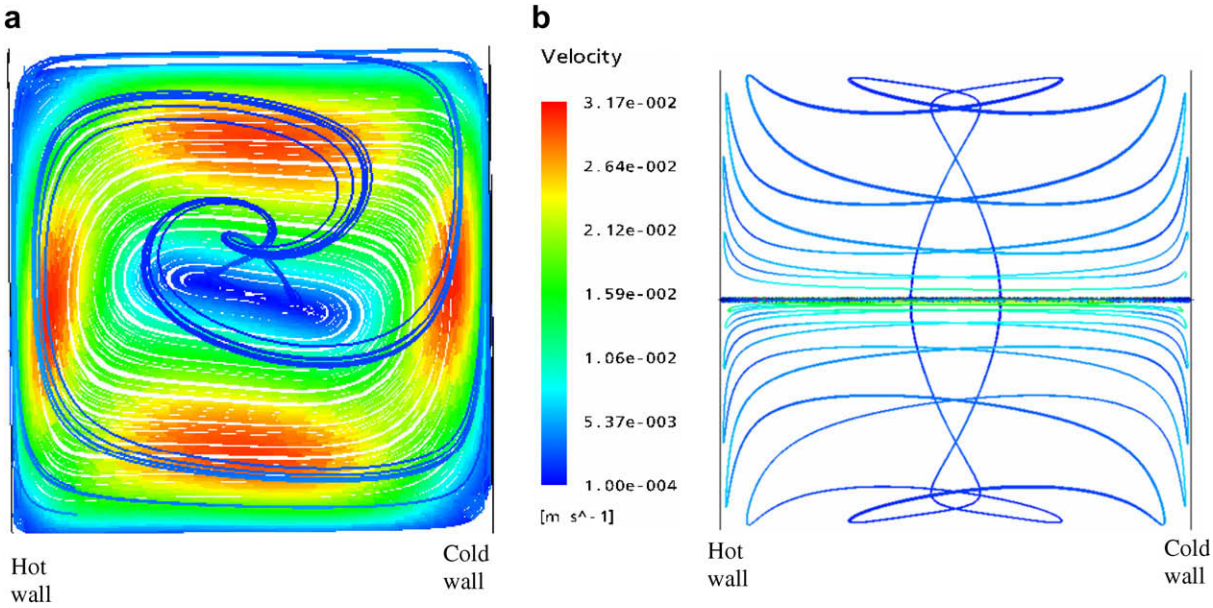

Fig. 9. Flow patterns in a horizontal cylinder at $Ra = 31027.47$. (a) Front view; (b) top view.

limited number of fluid paths are illustrated. The fluid converges to these two foci and circulates on the principal plane. They emerge from the principal plane and spiral upwards towards the hot and cold walls. At the walls the fluid is deflected even upwards and reaches eventually the curved walls where they begin to return towards the two foci. This is shown in Fig. 9b.

8.4. Cylinder inclined at 150°

For inclination angles less than 90°, on each side of the principal plane, there was only a single region of spiralling inward return flow. For the 90° case, even though two distinct loops were formed at the principal plane, they were not very far apart. Hence, the inward flow paths were quite close to each other. The two loops in the principal plane move further apart with increasing inclination angles past 90°. Due to this, two separate spiralling inward flow regions are evident even in the fluid bulk. This is shown in Fig. 10.

9. Regime classification

The ranges of Rayleigh numbers ($1034.25 \leqslant Ra \leqslant 31027.47$) and inclination angles ($0° \leqslant \alpha \leqslant 180°$) investigated in this work are

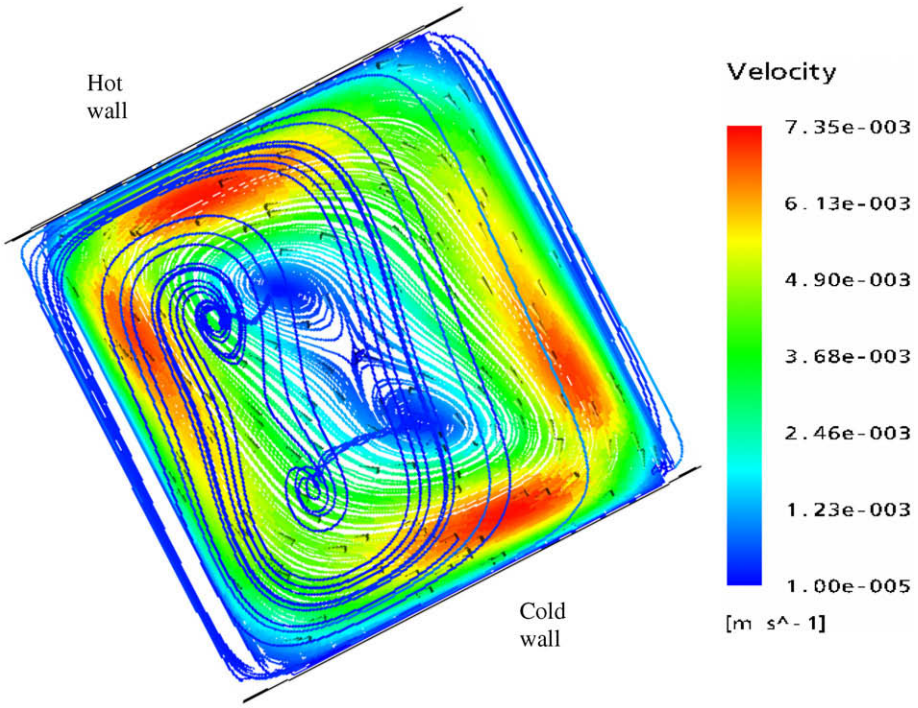

Fig. 10. Flow patterns in a 150° inclined cylinder at Ra = 31027.47.

classified into different regimes depending upon the effect of the natural convective flow on heat transfer. The trends exhibited by the vertical cylinder were quite different from those of the inclined cylinders. These differences may be observed in the Nusselt number (Fig. 11). It may be observed that the vertical cylinder trends fall in between the curves of 90° and 120°. This relatively poor performance in terms of heat transfer by the vertical cylinder when compared to the inclined cylinders may be mainly attributed to the requirement of a critical Rayleigh number of 3800. For inclination angles >0°, the numerical simulations indicated the convection to be observed even at very low Rayleigh numbers. Hence, the vertical and inclined cylinder cases were analysed separately.

The dimensionless axial temperature gradient (K) was utilized to classify the different flow regimes with respect to Rayleigh number and inclination angle. This approach is commonly used in the heat transfer literature [31,32]. It is defined as the ratio of the temperature gradient in the core to the actual temperature gradient imposed between the hot and cold walls ($\Delta T/L$)

$$K = -\frac{\frac{dT}{dz}}{\frac{\Delta T}{L}} \tag{10}$$

The variation of K with inclination angle and Rayleigh number is shown in Fig. 12. From this figure, different trends are evident even for inclined cylinders. For angles below 90°, the K values decrease rapidly with Rayleigh number and even become negative. However, for inclination angles >90°, the K values decrease slowly with Rayleigh number, become nearly constant and may even show a slight increase at high Rayleigh numbers. However, the horizontal cylinder exhibits trends that are similar to cylinders inclined beyond 90° at intermediate Rayleigh numbers (<20,000). Until this Rayleigh number, the K values are positive. However, for higher Rayleigh numbers (>25,000), the trend is similar to cylinders with inclination angles less than 90°. The Rayleigh number at which the K value becomes 0 is termed as

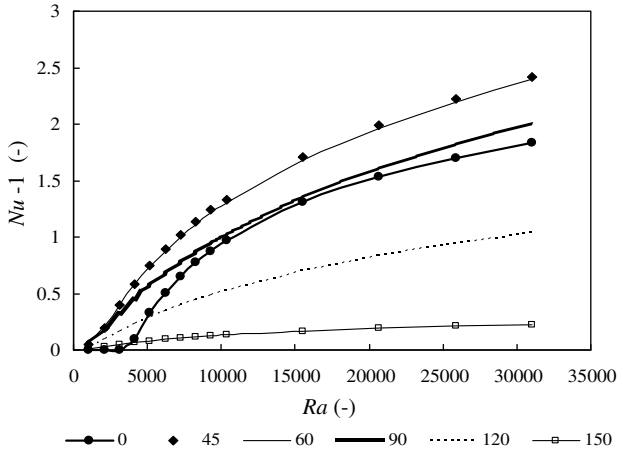

Fig. 11. Nusselt number trends at different inclination angles.

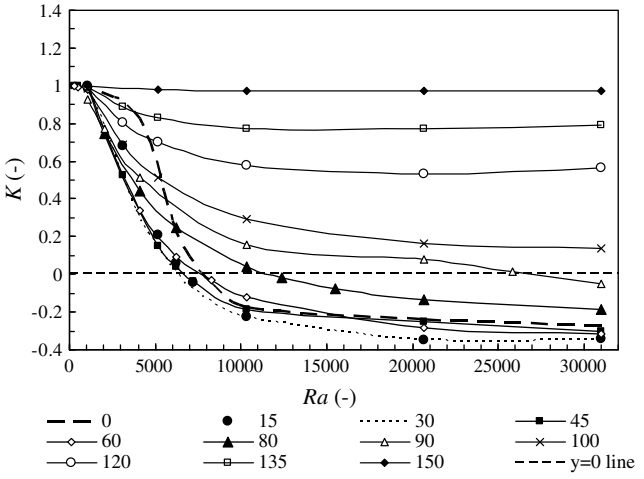

Fig. 12. Dimensionless axial temperature gradient as a function of inclination angle and Ra.

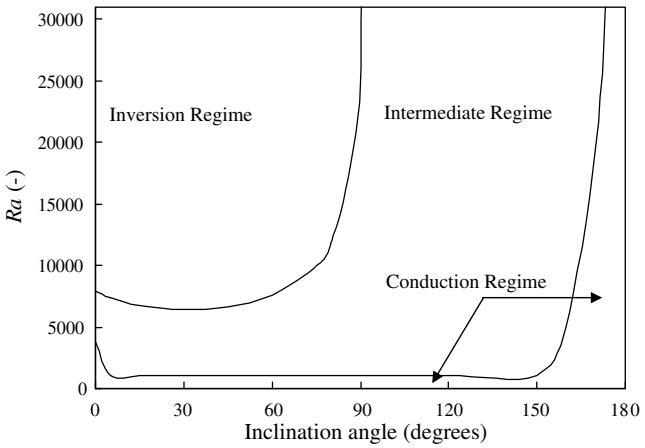

Fig. 13. Classification of flow regimes.

the transition Rayleigh number Ra_K. Based on these observations, the different flow regimes and their transition Rayleigh number (Ra_K) are shown in Fig. 13.

9.1. Conduction regime ($K \approx 1$)

This regime is characterized by mainly a linear axial temperature gradient.

9.1.1. Vertical cylinder

The conduction regime is the sub-critical regime ($Ra < 3800$).

9.1.2. Inclined cylinder ($0° < \alpha \leqslant 180°$)

For the inclined cylinder, convection is initiated almost immediately. But at very low Rayleigh numbers, the convection is less and the K values are still close to unity. Hence, for the inclined cylinders ($\alpha < 180°$), conduction regime was fixed until a maximum Rayleigh number of 1034.25. This corresponds to a temperature drop of 1 °C between the hot and cold walls. Even for inclination angles of 135° and 150°, the slight drop in K may be discerned in Fig. 12. For the 180° cylinder, the density gradient is stable and conduction is the only mechanism of heat transfer in entire Rayleigh number range investigated.

9.2. Intermediate regime ($0 < K < 1$)

In this regime, the hot fluid rises up and the cold fluid descends contributing to the fluid circulation. The axial transport of thermal energy due to convection currents will decrease the axial temperature gradient and the accompanying circulatory flow will increase the absolute value of the radial temperature gradient. In the intermediate regime, the K values decrease at the core with increasing Rayleigh number but are still positive.

9.2.1. Vertical cylinder

For this case, the Ra_K value was fixed at 7900. With further increase in Ra, the K values became negative.

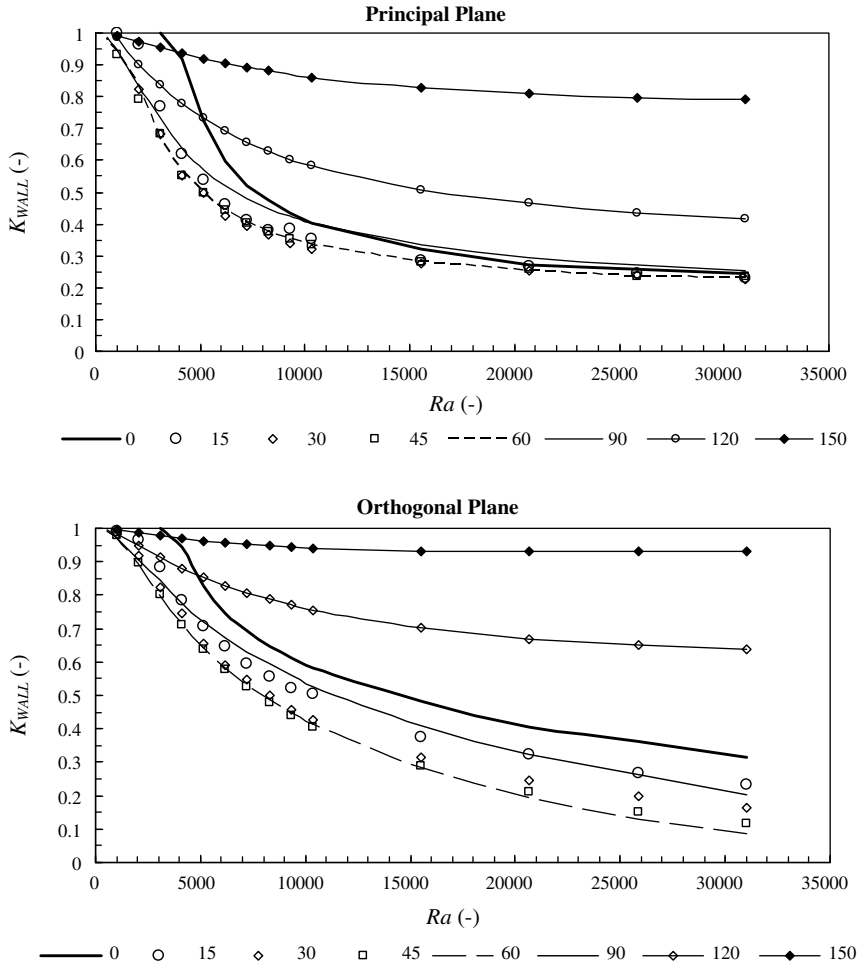

Fig. 14. Axial temperature gradient at the wall in the principal and orthogonal planes for different angles of inclinations.

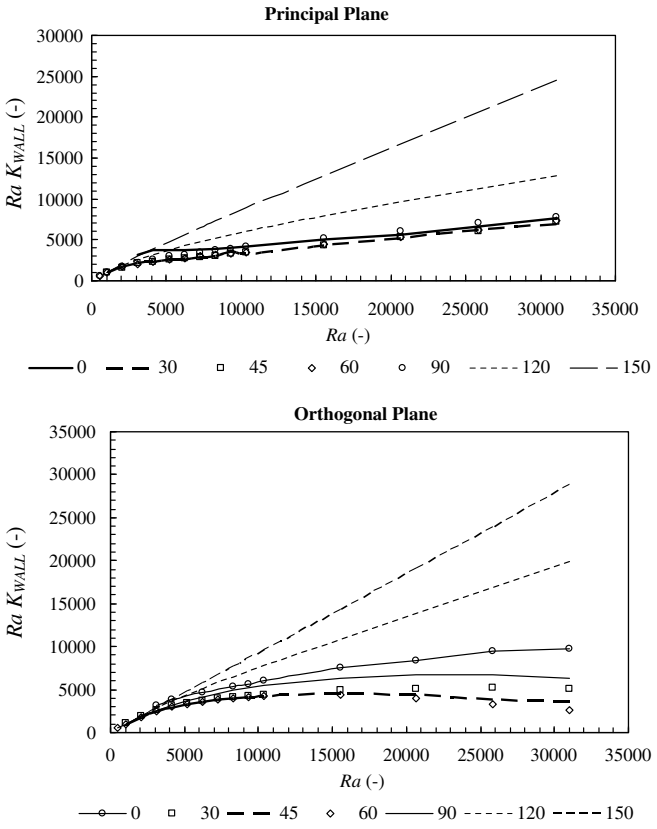

Fig. 15. Product of axial temperature gradient at the wall and Rayleigh number for different angles of inclinations.

9.2.2. Inclined cylinder ($0° < \alpha \leqslant 90°$)

For $\alpha \leqslant 90°$, Ra_K for the intermediate regime was dependent on the inclination angle. As the inclination angle increased from 0°, convection increased to a maximum leading to a rapid decrease in K (Fig. 12). The axial temperature gradient at the core became 0 in a relatively narrow Ra_K range for angles $0° < \alpha < 60°$. The Ra_K values for these angles were between 6500 and 7500. However, when the inclination angle was greater than 60°, the convection effects decreased and K decreased relatively more slowly with increasing Rayleigh number. This is shown for inclination angles 80° and 90° in Fig. 12. Based on inclination angles $0° < \alpha < 90°$, the criterion for identifying the transition Rayleigh number (Ra_K) was defined as

$$Ra_K \sin(\phi + 1.14) = 6.3 \quad (11)$$

where ϕ is the inclination angle in radians. At 90°, K became negative only at $Ra_K = 26{,}000$ and this was chosen as the transition Rayleigh number in Fig. 13.

9.2.3. Inclined cylinder ($90° < \alpha < 180°$)

Here, the flow regime over the entire range of Rayleigh number investigated (1034.25–31027.47) falls under the intermediate regime as the K values never become negative. A typical flow pattern involving a single loop at low Rayleigh numbers is shown in Fig. 16a. In this range of Ra, the K values decline with increasing Ra. At higher Rayleigh numbers, two loops form and the K values no longer decrease with Ra (Fig. 16b). Due to two loops formation; there is insufficient mixing in the core leading to more temperature stratification. In Fig. 17, the temperature contour plots are similar despite a Rayleigh number increase from 20,685 to 31027.47 for cylinder inclined at 120°. This may be compared with the temperature contour plot for the vertical cylinder (Fig. 18a) and 45° inclined cylinder (Fig. 23a). In the latter two figures, only a single loop is formed and more convection is evident at the highest Ra investigated.

9.3. Inversion regime ($K < 0$)

The negative value of K represents an inversion regime where the hot fluid begins to intrude into the upper regions of the cylinder. Similarly, the cold fluid also intrudes into the bottom region of the cylinder. This occurrence is shown for instance in Fig. 18(a). Hence, the axial temperature gradient in the core becomes negative. This is especially possible for unity aspect ratio cylinder where the distances traversed by the fluid along the vertical and horizontal directions are comparable.

9.4. Temperature gradient calculations at the adiabatic wall

For completeness, the dimensionless temperature gradient at the wall (K_{WALL}) was also calculated. Due to the asymmetric nature of the patterns, both the principal and orthogonal planes were considered. The results are shown in Fig. 14. In the principal plane, K_{WALL} increased only slightly with increasing inclination angle (between 0° and 90°) at the highest Ra value (31027.47) considered. However, results reported by Buscalioni and Crespo del Arco [31] at similar conditions but with cavity of aspect ratio 10 showed that K values increased at a higher rate especially at inclination angles greater than 50°. This indicates tendency towards thermal stratification with increasing inclination angles at higher aspect ratios. In the orthogonal plane for the unity aspect ratio cylinder, K_{WALL} values decreased with increasing inclination angles until 60°. However, for 90° the

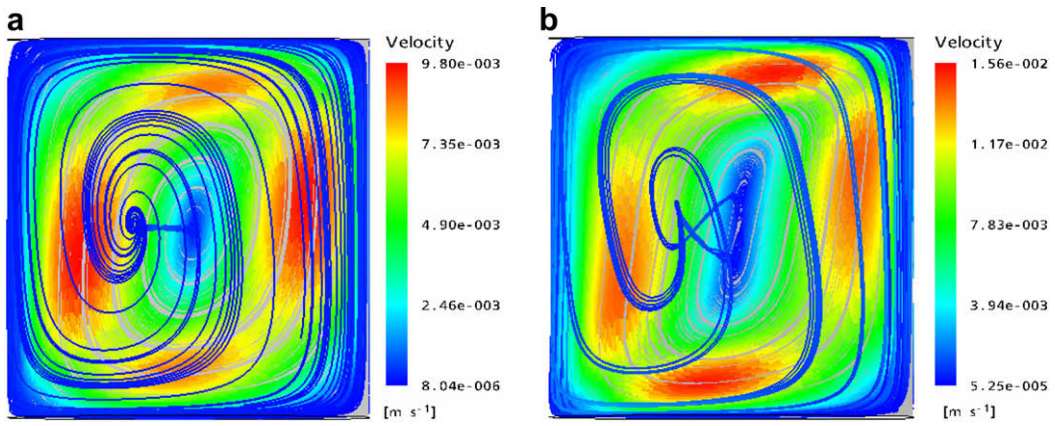

Fig. 16. Flow patterns in a 120° inclined cylinder. (a) $Ra = 7239.74$ and (b) $Ra = 20684.98$.

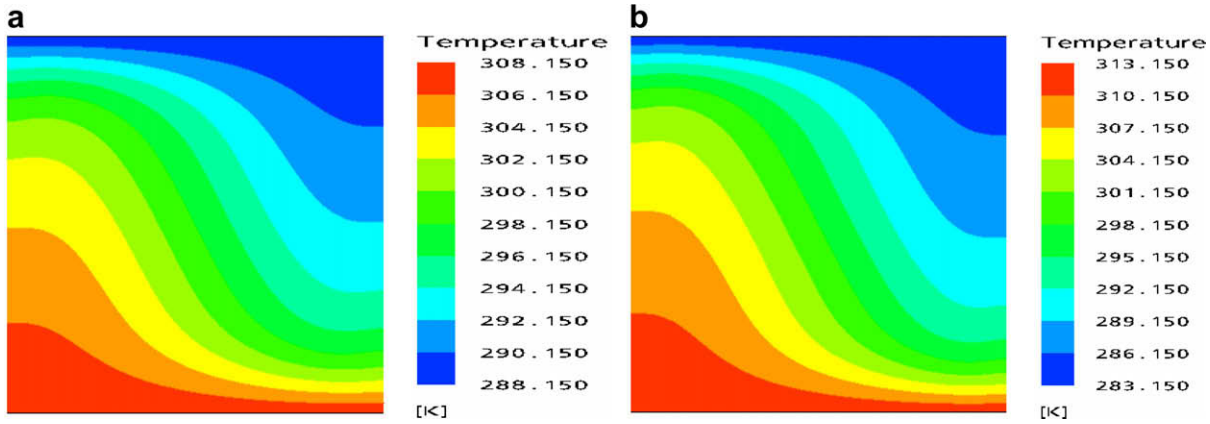

Fig. 17. Temperature contours in a 120° inclined cylinder. (a) Ra = 20684.98 and (b) Ra = 31027.47.

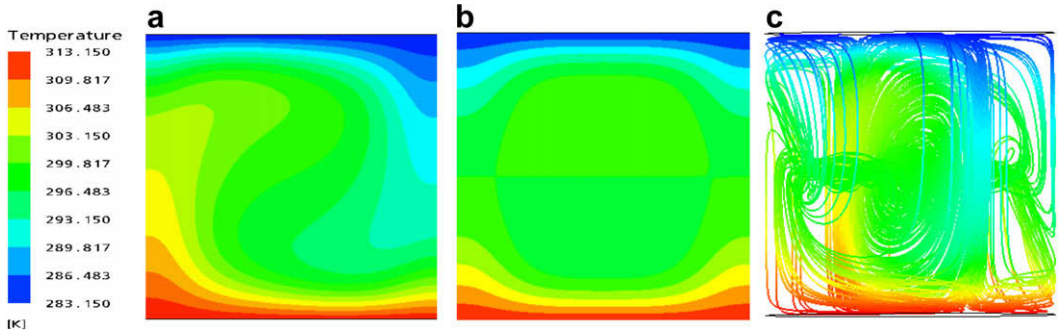

Fig. 18. Flow and temperature patterns in a vertical cylinder at Ra = 31027.47. (a) Temperature contour plot in the principal plane, (b) temperature contour plot in the orthogonal plane, and (c) flow paths labelled in terms of temperature.

K_{WALL} values, though exhibiting a declining trend with Ra, were higher than at 30° but lower than at 15°. This indicates that at high Rayleigh numbers there is relatively more convection near the walls of the orthogonal plane with increasing angles of inclination, provided they were below 90°.

The product of K_{WALL} and Ra is shown in Fig. 15. In the principal plane, this product is nearly independent of inclination angle over a wide range of values (0–90°) especially at higher Rayleigh numbers. This arises from the fact that the K_{WALL} itself is not very sensitive to both Ra and inclination angles below 90° at higher values of Rayleigh number (Fig. 14a). However, in the orthogonal plane there is distinct variation of RaK_{WALL} with inclination angles (0–90°) and at higher Ra, the RaK_{WALL} seems to even decrease. Since K_{WALL} decreases faster than the increase in Ra, there is a small reduction in $K_{WALL}Ra$ at higher Rayleigh numbers. This is in variance with the trends observed at the core for two-dimensional cavities at higher aspect ratios [31]. In two-dimensional cavities of high aspect ratios (7–100), the product of K_{WALL} and Ra tended asymptotically towards a limiting value. However, even in such cases, the lower the aspect ratio of the cavity, the slower RaK_{WALL} seemed to tend towards the limiting value.

10. Nusselt number analysis

At steady state, the area averaged Nusselt numbers (Nu) are the same irrespective of whether the area averaged heat flux ($\bar{q}$) is estimated at the cold or hot surfaces as there is no heat loss/gain through the adiabatic curved surface. This was also verified from the CFD simulation results.

10.1. Local Nusselt numbers (Nu_{loc})

The local Nusselt numbers (Nu_{loc}) were calculated in terms of the local heat fluxes using Eq. (9). Nu_{loc} were estimated along the bottom edges of the principal $(0,\pi)$ and orthogonal $(\pi/2,3\pi/2)$ planes for different inclination angles and results are presented in Fig. 19. The maximum in the local Nusselt number for the principal plane is shifted to the right. The hot fluid ascends along one side and penetrates into the region adjacent to the cold wall while the cold fluid descending from the top penetrates into the region adjacent to the hot wall (Fig. 18a). The thermal gradients are higher in the right-hand side where the cold fluid penetrates into the hotter region when compared to the left-hand side where the hot fluid ascends. Similarly, an off-centred maximum in local Nusselt numbers would have been shifted to the left if the calculations had been carried out along the top edge of the principal plane. Again, this would be due to penetration of the hot fluid into the cold region.

However, Nu_{loc} trends are symmetrical along the orthogonal plane with a maximum at the centre (Fig. 19b). The steeper thermal gradients at the middle of the top and bottom edges of the orthogonal plane (Fig. 18b) lead to the maximum of Nu_{loc} in the centre. The orthogonal plane shows a more uniform thermal core with temperature variations being restricted to the top and bottom edges. There is more mixing owing to hot fluid moving away from the bottom of the principal plane, ascending to the cold region and returning to the central region of the principal plane by traversing across the orthogonal plane in a spiralling fashion (Fig. 7). Similar behaviour is shown by the cold fluid. These are illustrated in fluid flow paths which are now labelled in terms of temperatures (Fig. 18c).

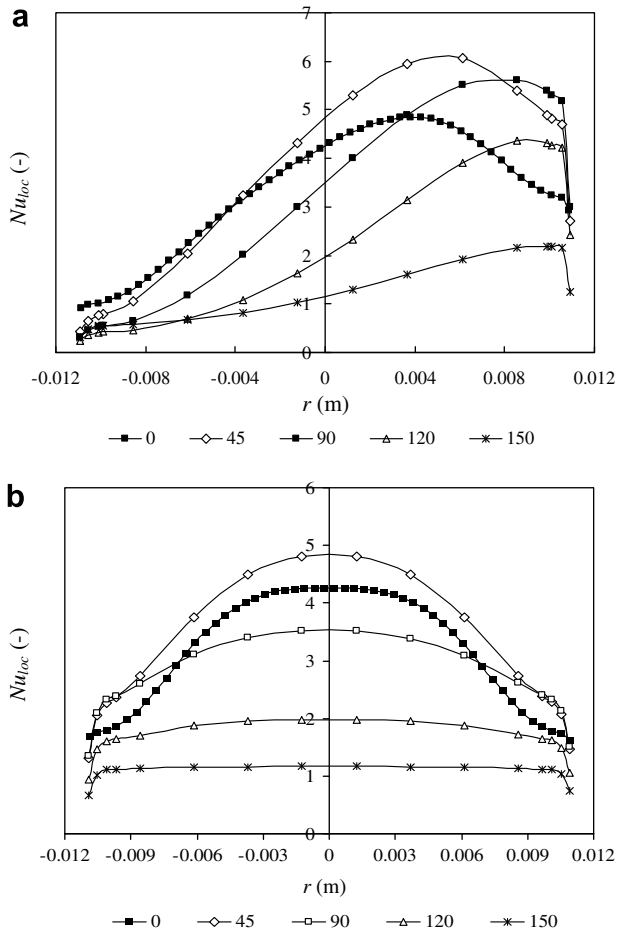

Fig. 19. Local Nusselt number variation along the radial direction at Ra = 31027.47. (a) Principal plane and (b) orthogonal plane.

As the inclination angles increase beyond 45°, the local Nusselt numbers tend to reduce as well as even out. These may be attributed to the growth of the thermal stratification layer from the top and bottom walls at the expense of the shrinking core region. In Fig. 20, the plots are given for the horizontal cylinder. In this figure, it may be seen that the vertical intrusions have declined in the principal plane (Fig. 20a). The thermal stratification layers at the top and bottom walls have thickened in the orthogonal plane (Fig. 20b). These lead to lower local Nu values. Fig. 20c shows that two loops have formed.

At inclination angles closer to 180°, conduction becomes the dominant heat transfer mechanism. As shown in Fig. 21a, the hot and cold fronts no longer penetrated to a considerable extent into the cold and hot regions as was observed for inclination angles less than or equal to 90° (Figs. 18 and 20) owing to declining of velocities by about an order of magnitude. Stratification is even more in the orthogonal plane (Fig. 21b). For angles of inclination beyond 90°, the two vortex centres have moved apart and there are two inward flows towards these vortex centres (Fig. 21c). This separation of the vortex centres lead to stratification of temperatures in the core of the orthogonal plane. This is in contrast to the flow patterns observed for inclination angles <90° where there was only a single vortex centre and the fluid streams from above and below took a common path towards the centre of the principal plane (Fig. 18c).

10.2. Maximum dimensionless velocity

The average Nusselt numbers follow a similar trend as that of maximum velocity in the domain (Fig. 24) with the occurrence of an optimum at an intermediate inclination angle. Hence, the maximum velocities in the domain were also analysed. The maximum dimensionless velocity in the domain was defined as follows:

$$V_{d,max} = V_{max}\frac{D}{\alpha_T} \tag{12}$$

The maximum value of velocity in the domain was determined by identifying surfaces with the highest constant velocity. The velocity value was reduced slowly from an arbitrarily high value until a sufficiently significant extent of region with the specified velocity was obtained. This method did not lead to any ambiguity in the identified maximum velocities. The iso-surface is sufficiently large and well inside the boundary, implying that this velocity value would significantly influence the main domain flow.

11. Correlations

The Nusselt number and maximum velocity correlations for the various regimes identified in Section 9 are presented in Table 2. The fit of the correlations to the CFD estimated Nusselt numbers and maximum velocities were within ±15%. The trends are discussed below.

11.1. Vertical cylinder

A reduced Rayleigh number for the vertical cylinder (Ra_{rv}) is defined by scaling with the critical Rayleigh number

$$Ra_{rv} = \frac{\text{Rayleigh number}}{3800} \tag{13}$$

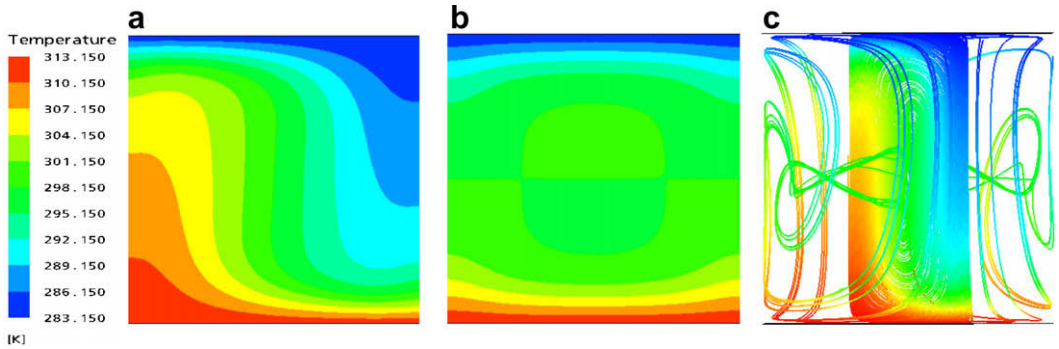

Fig. 20. Flow and temperature patterns in a horizontal cylinder at Ra = 31027.47. (a) Temperature contour plot in the principal plane, (b) temperature contour plot in the orthogonal plane, and (c) flow paths labelled in terms of temperature.

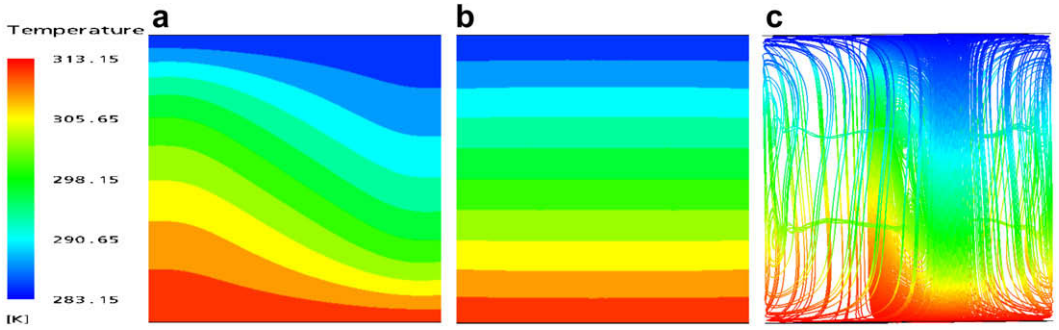

Fig. 21. Flow and temperature patterns in a cylinder inclined at $\alpha = 150°$ and $Ra = 31027.47$. (a) Principal plane, (b) orthogonal plane, and (c) flow paths labelled in terms of temperature.

Table 2
Correlations for maximum velocity and Nusselt number for the different regimes

Serial number	Regime	Range of application	Correlation
1	Vertical intermediate	$3800 < Ra \leqslant 7900$	$Nu = 1 + 0.71(Ra_{rv} - 1)^{0.77}$; $V_{d,max} = 16.66(Ra_{rv} - 1)^{0.48}$
2	Vertical inversion	$7900 < Ra \leqslant 31{,}027$	$Nu = 1.38(Ra_{rv})^{0.35}$; $V_{d,max} = 11.4(Ra_{rv})^{0.61}$
3	Inclined intermediate $0° < \alpha < 90°$	$1034 < Ra \leqslant Ra_K$	$Nu = 0.78(Ra_{ri})^{0.36}(1.36\sin\phi + \cos\phi)^{0.46}$; $V_{d,max} = 2.27(Ra_{ri})^{0.92}(0.98\sin\phi + \cos\phi)^{1.40}$
4	Inclined inversion $0° < \alpha < 90°$	$Ra_K < Ra \leqslant 31{,}027$	$Nu = 0.86(Ra_{ri})^{0.36}(1.11\sin\phi + \cos\phi)^{0.43}$; $V_{d,max} = 5.43(Ra_{ri})^{0.60}(0.7\sin\phi + \cos\phi)^{0.85}$
5	Horizontal ($\alpha = 90°$)	$1034 < Ra \leqslant 31{,}027$	$Nu = 0.915(Ra_{ri})^{0.35}$; $V_{d,max} = 5.21(Ra_{ri})^{0.53}$
6	Inclined intermediate $90° < \alpha \leqslant 180°$	$1034 < Ra \leqslant 31{,}027$	$Nu = 1 + 0.086(Ra_{ri})^{0.71}(\pi - \phi)^{1.90}$; $V_{d,max} = 3.37(Ra_{ri})^{0.49}(\pi - \phi)^{1.24}$

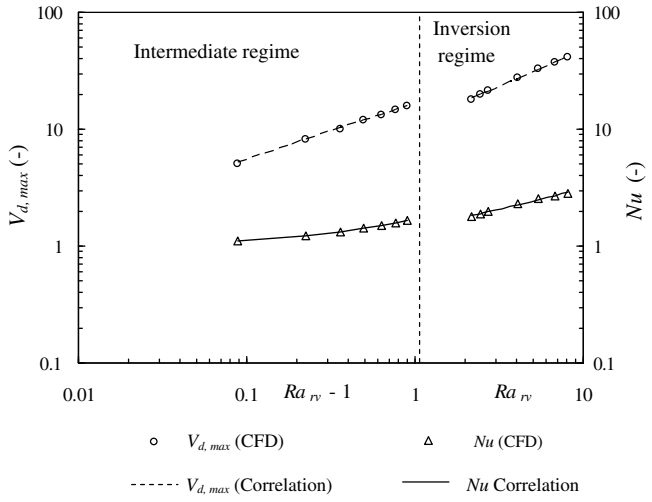

Fig. 22. Comparison of CFD data with correlations for the vertical cylinder in the intermediate and inversion regimes. Correlations are given in Table 2.

For sub critical Rayleigh numbers ($Ra_{rv} < 1$), the conduction heat transfer regime applies and the Nusselt numbers will be unity. The intermediate and inversion regimes apply in the Rayleigh number range 3800–7900 and $Ra > 7900$, respectively, as discussed in Section 9.2.1. The $V_{d,max}$ and Nu correlations for these regimes are given in Table 2. The fit of these correlations to the CFD data are shown in Fig. 22.

11.2. Inclined cylinder ($0° < \alpha < 90°$)

In these cases the Rayleigh numbers were scaled by dividing with the minimum value considered for transition from conduction dominated regime, i.e. 1034.25

$$Ra_{ri} = Ra/1034.25 \tag{14}$$

The temperature driving force increases with Rayleigh number leading to higher maximum velocity values. $V_{d,max}$ increases with inclination angle and passes through a maximum value around 45° in the intermediate regime and around 35° in the inversion regime. As shown in Figs. 7–10 and 23b the maximum velocities oc-

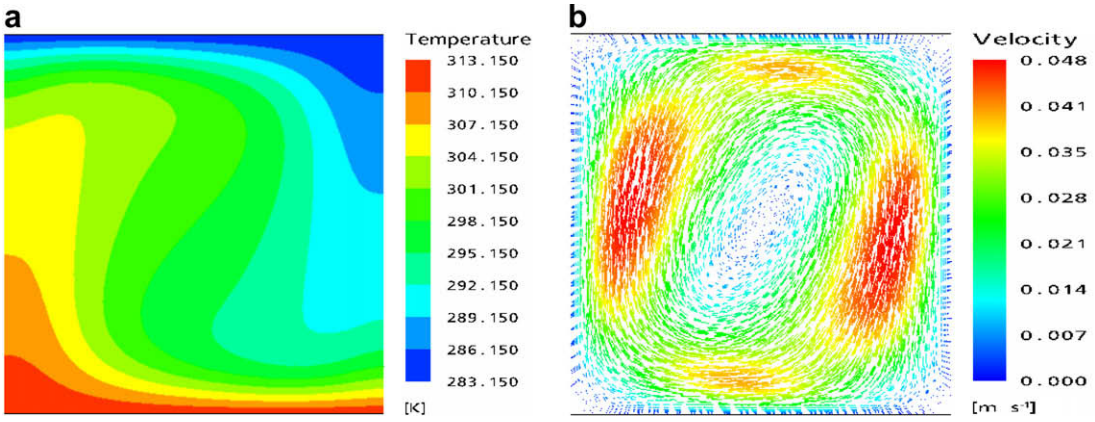

Fig. 23. Inversion regime characteristics for a cylinder inclined at 45° at $Ra = 31027.47$. (a) Temperature contour plot and (b) velocity vector plot.

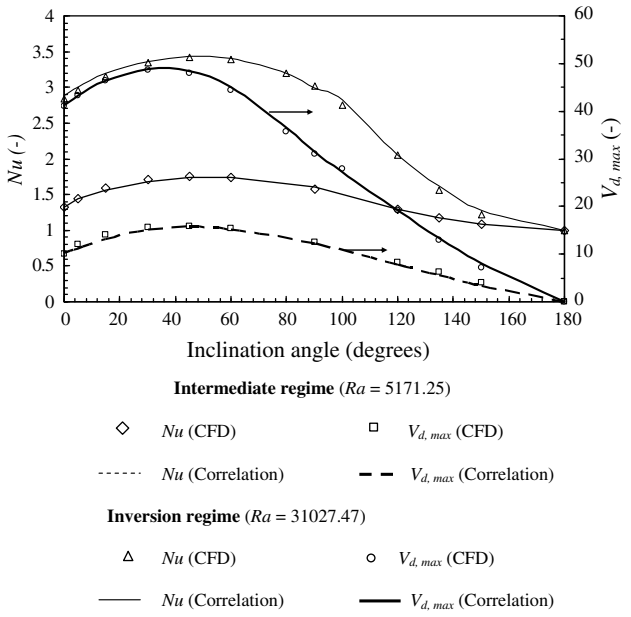

Fig. 24. Nusselt number and maximum velocity trends as a function of inclination angle. Correlations are given in Table 2.

cur close to the vertical and horizontal walls. Higher the vertical component of the velocity, more will the thermal energy penetrate into the colder region. The horizontal velocity will contribute to the thinning of the thermal stratification layers close to the top and bottom walls in the orthogonal plane (compare Figs. 18b, 20b, 21b and 23b). This will enable an overall increase in the Nusselt numbers. Therefore, the Nusselt number also increases with inclination angle and passes through a maximum around 54° in the intermediate regime and around 48° in the inversion regime. A more detailed discussion is presented in Section 12. The correlation predictions are compared with CFD results in Fig. 24. Both the radial and axial components of the buoyancy forces influence the Nusselt numbers and maximum velocities as may be observed from the coefficients of the $\sin(\phi)$ and $\cos(\phi)$ terms in the correlations.

11.3. Horizontal cylinder ($\alpha = 90°$)

Since the axial temperature gradient (K) profile had a trend that was distinctly different from those for cylinders inclined at angles <90°, it was decided to treat this case separately (Table 2). As the inversion regime occurs only at Ra close to the maximum value investigated as shown in Fig. 12 it was decided to develop correlations covering the entire Rayleigh number range.

11.4. Inclined cylinder ($90° < \alpha \leqslant 180°$)

In accordance with other inclination angles $0° < \alpha \leqslant 90°$, Rayleigh numbers were again scaled by using Eq. (14). Convective flow decreases with inclination angles >90° and finally the conduction mode of heat transfer is reached at 180°. The velocity values tend to 0 for an inclination angle of 180° irrespective of the Rayleigh number owing to the establishment of the stable density gradient. At this inclination angle, Nusselt number becomes unity (Fig. 24). In this figure, both Nu and $V_{d,max}$ are seen to be more sensitive to Ra for inclination angles below 90°. The reasons for this were discussed in Section 9.2.3.

11.5. Scaling relations for Nusselt number with Rayleigh number

As presented in Table 2, at higher Rayleigh numbers, the Nusselt number is proportional to Ra^n where the exponent n is about 0.35. Based on two-dimensional calculations with similar boundary conditions, Roux et al. [33] reported n to be 0.3 for horizontally oriented square cavities in the range $10^4 < Ra < 10^5$. The exponent was estimated as 0.29 from two-dimensional studies at high Rayleigh numbers on rectangular cavities inclined at angles below 90° [31]. For the situations discussed in the present study, there is more convection of heat in cylindrical enclosures when compared to two-dimensional rectangular enclosures.

12. Maximum Nusselt number at high Rayleigh numbers

As discussed in Section 11.2 and illustrated in Fig. 24, the maximum velocities in the domain and Nusselt numbers occur at different inclination angles. To analyse this difference, the velocities and convective fluxes were compared along a representative horizontal line constructed at the middle of the principal plane. The axial velocity component (w) was also scaled in accordance with Eq. (12). The axial convective flux was scaled with the overall conductive flux (q_k) across the cylinder as shown below to yield the dimensionless axial convective flux q_z^*

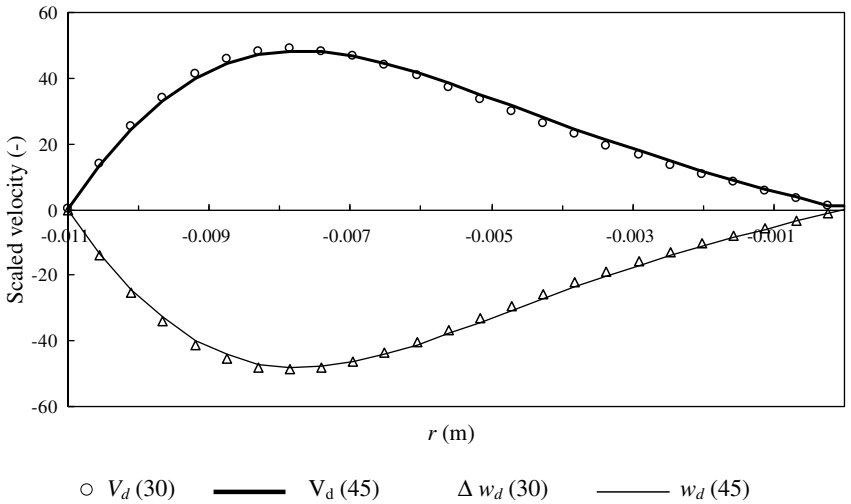

Fig. 25. Scaled velocities at the middle of the principal plane for cylinder inclined at 30° and 45° (Ra = 31027.47).

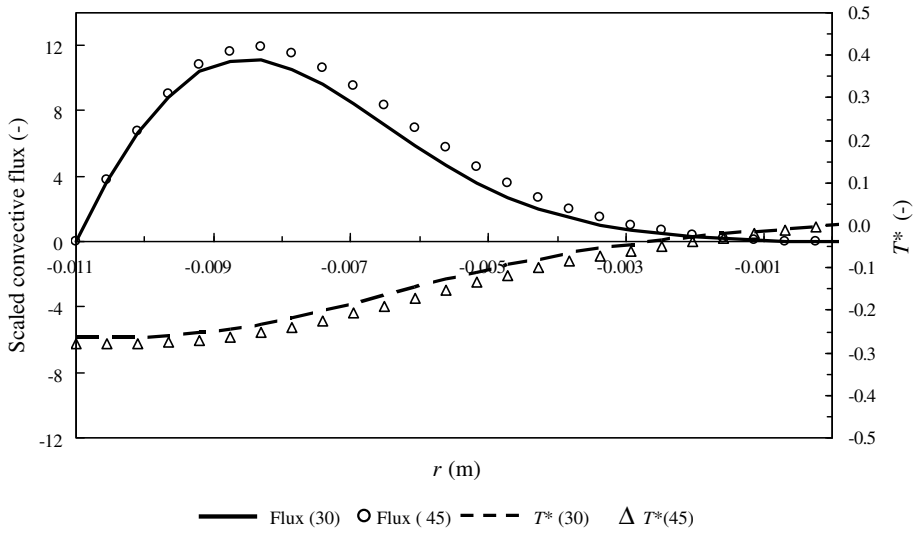

Fig. 26. Scaled convective fluxes and temperatures at the middle of the principal plane for cylinders inclined at 30° and 45° (Ra = 31027.47).

$$q_z^* = \frac{w\rho C_p(T - T_{\text{ref}})}{q_k} \tag{15}$$

where q_k is defined as follows:

$$q_k = \frac{k(T_{\text{hot}} - T_{\text{cold}})}{L} \tag{16}$$

T_{ref} refers to average of the hot and cold wall temperatures (in K). The temperature was also scaled as follows to range between −0.5 and 0.5.

$$T^* = \frac{(T - T_{\text{ref}})}{(T_{\text{hot}} - T_{\text{cold}})}$$

In Fig. 25, the axial velocities were compared for inclination angles 30° and 45° for the left half segment of the representative horizontal line on the principal plane. This corresponds to the descending cold fluid. Similarly, the axial convective flux and scaled temperatures were compared in Fig. 26. Typically, in the principal plane, even though the *maximum* overall velocity was higher for 30° than for 45°, it was not generally the case at other points as well. In some locations, the axial velocities were found to be slightly higher at 45° than at 30° (Fig. 25). It may be seen from Fig. 26 that the temperature driving force for convection will also be higher in the case of the 45° inclined cylinder thereby augmenting the effect of axial velocity component effect in increasing the axial convective transport. The Nusselt number, which is strongly influenced by the axial transport of the cold fluid from the top to the bottom region and correspondingly the axial transport of the hot fluid from the bottom to the top region, is hence higher for 45° cylinder inclination.

These findings were also compared with those of Crespo del Arco and Buscalioni [31] for inclined two-dimensional rectangular cavities of high aspect ratios and high Rayleigh number conditions. In their work, the Nusselt number was shown to be a function of the maximum axial velocity and the cross-stream temperature difference. The study revealed that while the maximum axial velocity occurred around 30° inclination similar to this study, the maximum in Nusselt number was found to occur close to 79°. In inclined rectangular cavities, the cross-stream temperature difference increased significantly for angles close to 90° [31]. Nearly a 2.9 times increase was observed at angles close to 90° relative to those observed at angles close to 30°. Their power law relationship showed a square root dependency of Nusselt number on maximum axial velocity and a linear dependency on cross-stream temperature difference. Due to a higher effect of the cross-stream temperature difference, the net result was to push the Nu values towards 79°. A qualitative comparison was made with the results from this study. It was observed that for the maximum Ra value (31027.47) investigated in this study, cross-stream temperature differences increased only slowly with inclination angle and the value at 90° inclination was only 1.2 times higher than at 30°. Hence, the net effect may be expected to be weaker for the cross-stream temperature difference in influencing the angle at

Table 3
Properties of helium used in the simulations

Serial number	Property	Value
1	Density (ρ)	0.179 kg/m^3
2	Viscosity (μ)	1.86×10^{-5} Pa s
3	Thermal conductivity (k)	1.42×10^{-1} W/(m K)
4	Specific heat (C_p)	5.240×10^3 J/(kg K)
5	Thermal expansivity (β)	0.00366 K^{-1}
6	Thermal diffusivity ($\alpha_T = k/(\rho C_P)$)	1.5086×10^{-4} m^2/s
7	Kinematic viscosity ($\nu = \mu/\rho$)	1.03911×10^{-4} m^2/s
8	Prandtl number ($Pr = C_p\mu/k$)	0.68

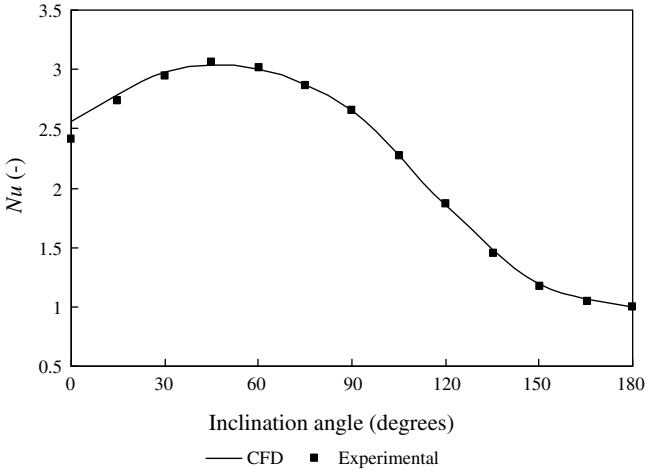

Fig. 27. Comparison of Nusselt number from CFD simulations with experimental data for helium at a Rayleigh number of 21,500.

which the maximum Nusselt number occurs in cylinders at low aspect ratios when compared to those for inclined two-dimensional rectangular cavities.

13. Validation of CFD simulations with available experimental results on Nusselt number

Schneider and Straub [16] also studied experimentally the effect of inclination on natural convection in inclined cylinder of unity aspect ratio. Helium ($Pr = 0.68$) was used as the test system and the cylinder length and height were fixed at 65 mm. The Rayleigh number was fixed at 21,500 using a temperature of 290.24 K at the hot wall and 256.06 K at the cold wall. The curved walls were made adiabatic. The details of the system studied are shown in Table 3. In the simulations of this study, a reference temperature of 273.15 K was used. The experimental Nusselt numbers obtained by Schneider and Straub [16] compare favourably with current CFD simulation values in Fig. 27. In addition, the relatively low values of Nusselt numbers obtained and their match with the experimental data validate the laminar flow model assumption.

14. Conclusions

The flow patterns induced by natural convection were three dimensional and sensitive to the inclination angle. There was more heat transfer for inclination angles in the range of 45–60°. For inclination angles beyond 90°, the hydrodynamics of the flow changed from a single vortex to a double vortex pattern. This occurrence as well as the declining radial and axial velocities has a strong effect on reducing the heat transfer rate. The local Nusselt number variation along the principal plane edge was asymmetric while it was symmetric along the orthogonal plane edge. Increasing Rayleigh number only had a relatively smaller heat transfer enhancement at inclination angles >90° when compared to those below 90°. At 180°, all flow patterns die out, and imply that heat transfer occurs by pure conduction only.

Acknowledgements

The simulations were carried out using the facility provided by Computational Fluid Dynamics Centre, IIT Madras. We are also grateful to the useful comments and suggestions from Dr. Arunn Narasimhan of Mechanical Engineering Department as well those from anonymous reviewers.

References

[1] C.F. Hess, C.W. Miller, Natural convection in a vertical cylinder subject to constant heat flux, Int. J. Heat Mass Transfer 22 (1979) 421–430.
[2] Y.S. Lin, R.G. Akins, Thermal description of pseudo-steady-state natural convection inside a vertical cylinder, Int. J. Heat Mass Transfer 29 (1986) 301–307.
[3] S. Ostrach, Natural convection in enclosures, J. Heat Transfer 110 (1988) 1175–1190.
[4] M. Varma, A. Kannan, Enhanced food sterilization through inclination of the container walls and geometry modifications, Int. J. Heat Mass Transfer 48 (2005) 3753–3762.
[5] R.G. Rice, M.A. Littlefield, Dispersion coefficients for ideal bubbly flow in truly vertical bubble columns, Chem. Eng. Sci. 42 (1987) 2045–2053.
[6] M.H.I. Baird, K. Aravamudan, N.V. Rama Rao, J. Chadam, A.P. Peirce, Unsteady axial mixing by natural convection in a vertical column, AIChe J. 38 (1992) 1825–1834.
[7] H. Ozoe, K. Yamamoto, H. Sayama, S.W. Churchill, Natural convection in an inclined rectangular channel heated on one side and cooled on the opposing side, Int. J. Heat Mass Transfer 17 (1974) 401–406.
[8] J.N. Arnold, I. Catton, D.K. Edwards, Experimental investigation of natural convection in inclined rectangular regions of differing aspect ratios, J. Heat Transfer 98 (1976) 67–71.
[9] W.M.M. Shinkel, Natural Convection in Inclined Air Filled Enclosures, Dutch Efficiency Bureau, Pijnacker, 1980.
[10] C.Y. Soong, P.Y. Tzeng, D.C. Chiang, T.S. Sheu, Numerical study on mode-transition of natural convection in differentially heated inclined enclosures, Int. J. Heat Mass Transfer 39 (1996) 2869–2882.
[11] R.A. Kuyper, Th. H. Van Der Meer, C.J. Hoogendoorn, R.A.W. M Henkes, Numerical study of laminar and turbulent natural convection in an inclined square cavity, Int. J. Heat Mass Transfer 36 (1993) 2899–2911.
[12] P. Bontoux, C. Smutek, A. Randriamampianina, B. Roux, G.P. Extremet, A.C. Hurford, F. Rosenberger, G. de Vahl Davis, Numerical solutions and experimental results for three-dimensional buoyancy driven flows in tilted cylinder, Adv. Space Res. 6 (1986) 155–160.
[13] A. Heiss, S. Schneider, J. Straub, g-Jitter effects on natural convection in a cylinder: three-dimensional numerical calculations, in: Proceedings of the Sixth European Symposium on Material Sciences under Microgravity Conditions, Bordeaux (ESA SP-256), 1986, pp. 517–523.
[14] G. Neumann, Three-dimensional numerical simulation of buoyancy driven convection in vertical cylinders heated from below, J. Fluid Mech. 214 (1990) 559–578.
[15] E. Crespo del Arco, P. Bontoux, R.L. Sani, G. Hardin, G.P. Extremet, Steady and oscillatory convection in vertical cylinders heated from below, Numerical simulation of asymmetric flow regimes, Adv. Space Res. 8 (1988) 281–292.
[16] S. Schneider, J. Straub, Laminar natural convection in a cylindrical enclosure with different end temperatures, Int. J. Heat Mass Transfer 35 (1992) 545–557.
[17] G. Muller, G. Neumann, W. Weber, Natural convection in vertical Bridgman configurations, J. Cryst. Growth 70 (1984) 78–93.
[18] F. Heslot, B. Castaing, A. Libchaber, Transitions to turbulence in helium gas, Phys. Rev. A 36 (1987) 5870–5873.
[19] Y.L. He, W.Q. Tao, T.S. Zhao, Z.Q. Chen, Steady natural convection in a tilted long cylindrical envelope with lateral adiabatic surface. Part 2. Heat transfer rate, flow patterns and temperature distributions, Numer. Heat Transfer A 44 (2003) 399–431.
[20] C. Cianfrini, M. Corcione, P.P. Dell'Omo, Natural convection in tilted square cavities with differentially heated opposite walls, Int. J. Therm. Sci. 44 (2005) 441–451.
[21] C.J. Craig, V. Subramanyan, D.T. Valentine, On the convection in an enclosed container with unstable side wall temperature distributions, Int. J. Heat Mass Transfer 41 (1998) 2307–2320.
[22] M.C. D'Orazio, C. Cianfrini, M. Corcione, Rayleigh–Bénard convection in tall rectangular enclosures, Int. J. Therm. Sci. 43 (2004) 135–144.
[23] CFX Documentation, CFX Ltd., The Gemini Building, Harwell International Business Centre, Didcort, Oxfordshire OX11 OQR, UK, 2005.
[24] C.M. Rhie, W.L. Chow, Numerical study of the turbulent flow past an airfoil with trailing edge separation, AIAA J 21 (1983) 1527–1532.
[25] H. Wang, M.S. Hamed, Flow mode-transition of natural convection in inclined rectangular enclosures subjected to bidirectional temperature gradients, Int. J. Therm. Sci. 45 (2006) 782–795.
[26] G.S. Charlson, R.L. Sani, Thermo convective instability in a bounded cylindrical fluid layer, Int. J. Heat Mass Transfer 13 (1970) 1479–1496.
[27] G.S. Charlson, R.L. Sani, On thermo convective instability in a bounded cylindrical fluid layer, Int. J. Heat Mass Transfer 14 (1971) 2157–2160.
[28] J.C. Buell, I. Catton, The effect of wall conduction on the stability of a fluid in a right circular cylinder heated from below, J. Heat Transfer 105 (1983) 255–260.
[29] E. Crespo del Arco, P. Bontoux, Numerical solution and analysis of asymmetric convection in a vertical cylinder: an effect of Prandtl number, Phys. Fluids A 1 (1989) 1348–1359.
[30] P. Bontoux, C. Smutek, B. Roux, J.M. Lacroix, Three-dimensional buoyancy driven flows in cylindrical cavities with differentially heated end walls. Part 1. Horizontal cylinders, J. Fluid Mech. 169 (1986) 211–227.
[31] R.D. Buscalioni, E. Crespo del Arco, Flow and heat transfer regimes in inclined differentially heated cavities, Int. J. Heat Mass Transfer 44 (2001) 1947–1962.
[32] G. de Vahl Davis, Laminar natural convection in an enclosed rectangular cavity, Int. J. Heat Mass Transfer 11 (1968) 1675–1693.
[33] B. Roux, J.C. Grondin, P. Bontoux, B. Gilly, On a higher-order accurate method for the numerical study of natural convection in a vertical square cavity, Numer. Heat Transfer 1 (1978) 331–349.